Bull. Spec. Astrophys. Obs., 1996. 41. 5–27

Spectroscopic investigation of the PPN candidate AI CMi = IRAS 07331+0021

V.G. Klochkova, V.E. Panchuk

Special Astrophysical Observatory of the Russian AS, Nizhnij Arkhyz 357147, Russia

Received March 22, 1996; accepted March 25, 1996.

Abstract.
Chemical composition (26 elements) of the cool supergiant AI CMi was studied by the model atmosphere method using echelle spectra taken with the 6 m telescope in 1993–95. Metallicity of the star turns to be by an order of magnitude lower than solar, the abundance of α–process elements (Na, Mg, Al, Si) is on the average $[\alpha/\mathrm{Fe}] = 0.33$, the mean abundance of heavy s–process elements (La, Ce, Pr, Nd) is $[\mathrm{s/Fe}] = -0.35$. Together with the radial velocity determination results this permits us to classify AI CMi with halo population or with population of the old (thick) disk. The spectra obtained in 1994 and 1995 contain titanium oxide bands which allowed the outermost AI CMi atmosphere layer characteristics to be estimated. The presence of emission components in hydrogen lines of Balmer and Paschen series is indicative of mass loss with varying rate.

Key words: stars: evolution – stars: post – AGB – stars: individual: AI CMi

1. Introduction

This paper is another one from the series of those on investigation of stars, which are believed to be at the post–AGB stage (Klochkova, 1995; Zach et al., 1995, 1996; Klochkova et al., 1996). In the General Catalogue of Variable Stars (GCVS) (Kukarkin et al., 1969) AI CMi is classified as an irregular variable of L type ($m_{ph} = 8.8 \div 10.6$), possibly belonging to SRd or R CrB type. McConnel and Bidelmann (1976) classified the star as a supergiant G5Iab. Eggen (1983) included AI CMi in the list of pseudocepheids — massive supergiants from the Hertzsprung gap, whose spectra at classification dispersions are indistinguishable from the spectra of cepheids, but having brightness variations of lower stability. Two runs of medium band photometric observations revealed non–periodic brightness variations of a cycle less than 100 days, but the absence of a colour index and V brightness correlation and strong reddening did not permit the luminosity to be determined. In the fourth issue of GCVS (Kholopov et al., 1985) AI CMi, as before, is classified as an irregular variable (L:), but already without the comment "possibly SRd or R CrB". Luck and Bond (1989) classified it with low–mass variable supergiants. Using an echelle spectrum, recorded on a photoplate with the help of an image tube, they determined its chemical composition by the model atmosphere method. The obtained metallicity $[\mathrm{Fe/H}] = -1$ suggested that the star belongs to the halo or thick disk population. Apparently, with this metallicity MK classification gives an earlier spectral subclass, and results in overestimated T_{eff}.

The low metallicity, excess in the near IR region, its galactic coordinates and brightness variation behaviour allow AI CMi to be ranked among objects at the post–AGB stage, where a chemical composition anomaly and mass loss indications can be revealed with high probability.

2. Observations and reduction of spectrograms

Observations of AI CMi were carried out at the 6 m telescope with a high–resolution echelle spectrometer equipped with a CCD chip (Panchuk et al., 1993). Table 1 presents the observational log. The first three spectra were taken with a CCD of 530 × 580 pixels, and the fourth one — with the 1040 × 1160 pixels CCD. Each of the four observations represents two separate spectrum integrations, obtained sequentially with the same exposure time. Such procedure is needed to exclude cosmic particle traces. Echelle spectra were reduced using the MIDAS program package for echelle spectrum reduction (version NOV95), for separate spectral orders the program of Galazutdinov (1992) was used. The identification of spectral lines was performed taking into account the Luck (1991) and Meinel et al. (1969) lists. Titanium oxide bands

Table 1: *Observing log*

Date	Number of spectrum	Range $\lambda\lambda$(Å)	Spectral resolution R	V_r km/s	Notes
11.01.93	04106	5500-8780	25000	46.6	"hot" phase
12.03.93	04603	5500-8780	25000	48.4	"hot" phase
21.12.94	10207	5500-7200	25000		"cool" phase
11.12.95	13011	4630-6800	20000	49.6	"cool" phase

are seen in the third and fourth spectra, which explains the comments in Table 1. The first two spectra have hydroxyle emissions ($\lambda\lambda$ 6862, 8025, 8761, 8768 Å) and neon ($\lambda\lambda$ 6508, 7490 Å) in the IR range, in the fourth spectrum emission of the Earth's atmosphere is represented only by the weak auroral doublet near λ 5259 Å. Besides, in the first two spectra the weak emission lines $\lambda\lambda$ 7190, 7497, 7976, 8451 Å, characteristic for nova-like object spectra, are seen.

3. Radial velocities and equivalent widths

Radial velocities V_r measured from 50 absorption lines showed no statistically significant variations from spectrum to spectrum. Variations of radial velocities owing to the effective level of the atmosphere, where the line was formed, were not revealed either. Average values of radial velocities are given in Table 1. The equivalent widths W for the first, second and fourth spectra are given in Table 2. The third spectrum was taken with a long-focus camera in combination with the CCD chip of 530 × 580, i.e. without overlapping of the neighbouring orders of echelle spectrum. The presence of molecular bands did not permit the continuum level to be located and equivalent widths to be measured with any assurance. The fourth spectrum was taken with a short–focus camera combined with the 1040 × 1160 CCD, and continuum level is located reliably for all spectral orders. Because of the TiO bands in the "cool" phase (see Fig. 1), in the fourth spectrum we measured W of only the lines that fell in the "transparency windows". The oscillator strengths gf listed in Table 2 are from Luck (1991).

4. Atmosphere parameters and chemical composition

To determine the effective temperature T_{eff} and atmosphere gravity log g we used numerous lines of neutral iron and FeII measured from the first two spectrograms. T_{eff} was determined based on the equality of the iron abundance ε(Fe) obtained from lines of different low level excitation potentials χ_L. The microturbulent velocity ξ_t was determined provided that ε(Fe) is independent of W. The gravity log g was determined from equality of the mean values of ε(Fe) obtained from FeI and FeII lines. All the calculations were made using the Bell et al. (1976) model grid and its later unpublished extensions. The atmosphere parameters for the "cool" and "hot" phases are listed in Table 3, as well as the data of Luck and Bond (1989) for the photometric phase 50 days after the maximum, i.e. halfway between the maximum and minimum of the star brightness (Luck and Bond, following Eggen, suggest that the brightness variations of AI CMi are semiregular with a typical period of 80–100 days). Details of determining the atmosphere parameters for the "cool" phase are reported below.

For the parameters listed in Table 3 abundances of 26 chemical elements are calculated by the model atmosphere method from "cool" and "hot" phase spectra, the results are given in Table 4. In the head of Table 4 parameters of the adopted models are displayed. The number of spectral lines used for chemical composition calculation, n, is indicated. For the "cool" phase the number of the measured atomic lines is small because of blending with molecular spectrum details. The responsivity of chemical composition determination results to errors of determination of the atmosphere parameters for the given range of parameters is reported in Zach et al. (1995). The logarithmic differences $[X/Fe]_\odot$ are calculated relative to the chemical composition of the solar atmosphere (Grevesse, 1993), and for AI CMi at the "cool" phase only estimates of ε(Fe) from FeI lines were used.

5. AI CMi atmosphere structure features at "cool" phase

Let us consider in detail the interpretation of the AI CMi "cool" phase spectrum. At first empirical relationship between a spectral class and intensity discontinuities near TiO band heads will be used, then we will attempt to determine T_{vib}, temperatures, which characterize the Boltzmann population of TiO vibrational levels. Now numerical estimations will follow, which allow the region of formation of molecular spectrum in the atmosphere to be defined.

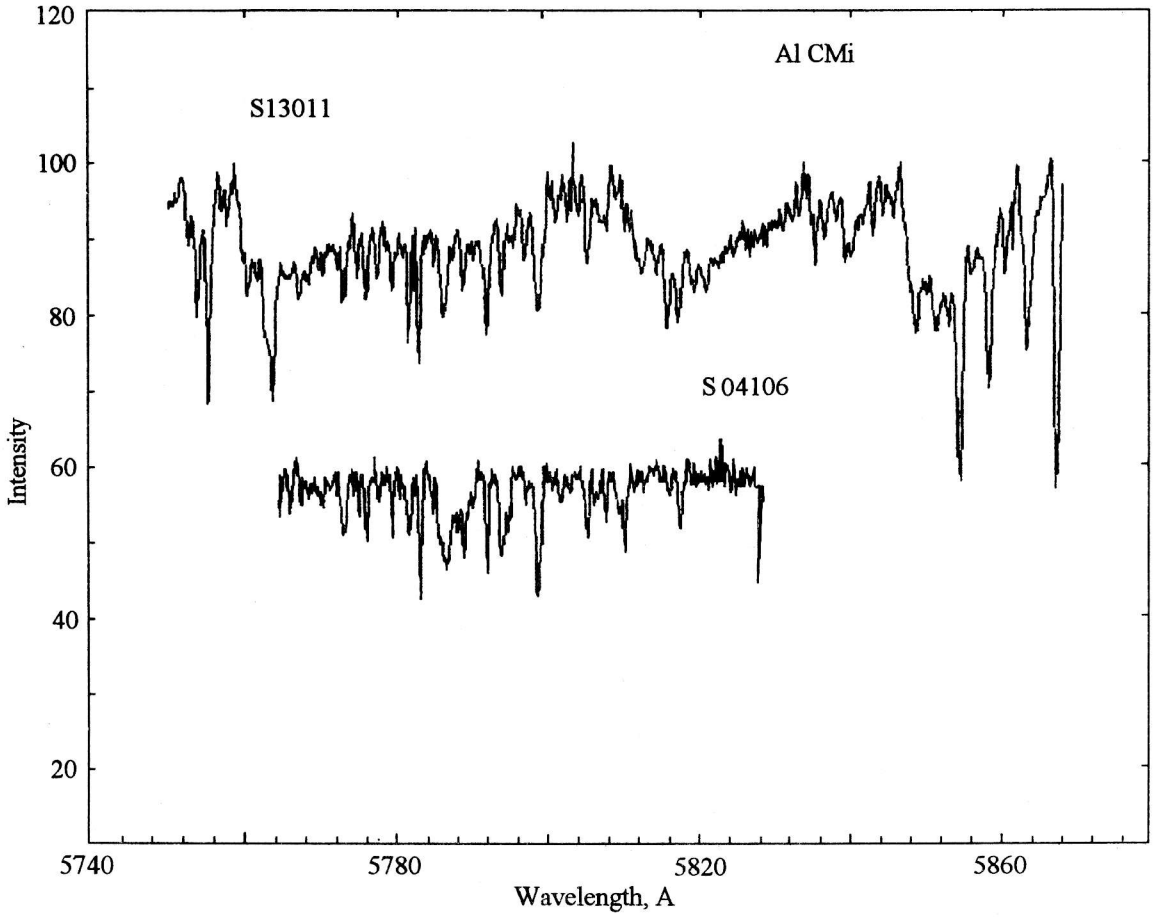

Figure 1: *Parts of echelle-orders showing the TiO band appearance.*

Table 3: *Model atmosphere parameters of AI CMi for different moments of the observation*

Date	T_{eff}	log g	ξ_t	[Fe/H]	Notes
24.02.81	4250	-0.8	4.0	-1.03	Luck and Bond (1989)
11.01.93	4500	0.0	3.0	-1.13	"hot phase"
12.03.93	4500	1.0	3.5	-1.19	"hot phase"
11.12.95	4100	-0.75	4.0	-1.03	"cool phase"

5.1. Sp and T_{eff} estimates from band head intensity jumps

The spectra of AI CMi taken on 21.12.94 and 11.12.95 exhibit titanium oxide bands (Fig. 1). Numerical modelling of the titanium oxide spectrum is associated with some uncertainties, therefore at first empirical estimation of AI CMi effective temperature on 11.12.95 must be performed. We estimate the atmosphere effective temperature from band head intensity jumps in the spectrum of TiO α-system, using the data of Boyarchuk (1969), where the band intensity jumps ($I_{\lambda+}/I_{\lambda-}$) are given as a function of spectral subclass M for giants. Unfortunately, the spectral resolution of the used data is not given in the paper of Boyarchuk (1969), which makes it difficult to compare them with our data. In the cited paper the spectra with a reciprocal linear dispersion of 80 Å/mm are used, that is why before the comparison we must evaluate how a change in spectral resolution affects the band head intensity jumps. We made convolution of intensity distribution in each spectral order with the instrumental profile $\Delta\lambda$ of different width, and measured band head intensity jumps as a function of the width. Examples of such relations are given in Fig. 2.

Table 4: *Chemical composition of AI CMi from different spectra (at* $\log\varepsilon(H) = 12.0$)

	$T_{eff} = 4500K, \log g = 0.0, \xi_t = 3.0$				$T_{eff} = 4500K, \log g = 1.0, \xi_t = 3.5$				$T_{eff} = 4100K, \log g = -0.75, \xi_t = 4.0$			
X	$-\log\varepsilon$	$\sigma\log\varepsilon$	n	$[X/Fe]_\odot$	$-\log\varepsilon$	$\sigma\log\varepsilon$	n	$[X/Fe]_\odot$	$-\log\varepsilon$	$\sigma\log\varepsilon$	n	$[X/Fe]_\odot$
LiI	11.96		1		11.65		1					
OI*					3.28		1	+1.04	3.46		1	+0.70
NaI	6.52	0.10	3	+0.28	6.68	0.14	2	+0.18	6.32	0.06	3	+0.38
MgI	5.05	0.18	5	+0.66	5.55	0.09	3	+0.06	5.28		1	+0.17
AlI	6.10	0.21	4	+0.56	6.67	0.02	2	+0.05				
SiI	5.14	0.28	26	+0.54	5.23	0.06	18	+0.41	5.08	0.12	4	+0.40
CaI	6.69	0.42	18	+0.08	6.88	0.05	8	-0.05	6.89	0.14	9	-0.22
ScII	10.59	0.28	8	-0.63	10.38	0.04	4	-0.36	9.55	0.17	6	+0.31
TiI	7.40	0.18	28	+0.29	7.64	0.04	18	-0.47	7.56	0.08	11	+0.55
TiII	8.70	0.08	2	-1.59	8.04		1	-0.87				
VI	8.74	0.20	21	+0.39	8.84	0.05	20	+0.35	8.84	0.13	3	+0.19
VII	9.56	0.23	4	+0.43	9.24	0.14	2	-0.05				
CrI	7.40	0.34	12	+0.06	7.66	0.10	6	-0.14	7.17	0.15	6	+0.19
MnI	8.25	0.02	3	-1.51	8.34	0.04	3	-1.54	7.54	0.00	2	-0.90
FeI	5.63	0.22	117		5.69	0.02	81		5.53	0.03	52	
FeII	5.73	0.23	41		5.63	0.12	8		5.33	0.08	2	
CoI	8.02	0.27	6	+0.19								
NiI	6.94	0.22	26	-0.06	7.00	0.05	18	-0.06				
CuI	9.12		1	-0.20	9.61		1	-0.63	8.80	0.24	2	+0.02
ZnI									7.83		1	+0.60
YI	10.34	0.47	3	+0.55					10.57		1	+0.22
YII	11.15		2	-0.26	10.41		1	+0.54	11.26	0.13	4	-0.47
ZrI	10.34	0.29	6	+0.19	10.40	0.14	3	+0.19	10.69	0.12	3	-0.26
ZrII									10.95		1	-0.52
MoI	10.63	0.02	3	+0.58	10.64		1	+0.63				
BaII	10.99	0.16	2	+0.01	11.08		1	-0.02	9.90	0.12	3	**
LaII	12.29	0.28	4	-0.38	11.82	0.10	4	+0.15	11.98	0.08	2	-0.17
CeII					12.49		1	-0.85	11.99		1	-0.51
PrII									12.89		1	-0.57
NdII	12.11	0.30	3	-0.48	11.04	0.18	2	+0.65	11.80	0.13	5	-0.27
EuII	2.62	0.42	2	0.00	12.33		1	+0.35	11.98	0.23	3	+0.54

* abundance of oxygen is based on forbidden line λ6300 Å

** in this spectrum BaII lines are very strong, with W > 380 mÅ

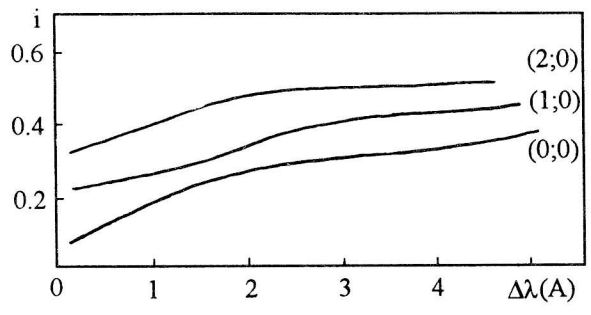

Figure 2: *Dependences* $i = I_{\lambda+}/I_{\lambda-}$ *on* $\Delta\lambda$ *for TiO α-system bands (0:0), (1:0), (2:0).*

Assume that the spectral resolution of Boyarchuk (1969) data is defined by photographic emulsion resolution (about 0.03 mm), then the spectral resolution is $\Delta\lambda = 80$ Å/mm × 0.03 mm = 2.4 Å. Using this value, we read i values from the relations similar to those plotted in Fig. 2. The results of the measurements are given in Table 5, where successively are given: wavelengths of the band heads, quantum numbers of the upper (ν') and lower (ν'') vibrational levels, Frank–Condon factors (q) from McCallum et al. (1970), conventional number of an order (N) in the fourth echelle spectrum of AI CMi, band head intensity jump values ($I_{\lambda+}/I_{\lambda-}$) for $\Delta\lambda = 2.4$ Å, and spectral subclass M obtained for the given ($I_{\lambda+}/I_{\lambda-}$) us-

ing the relationship between $(I_{\lambda+}/I_{\lambda-})$ and Sp published by Boyarchuk (1969). The last column of Table 5 presents subclass name obtained on the assumption that the spectral resolution of Boyarchuk (1969) data is lower by a factor of 1.5 of the value adopted. The mean spectral class then turns out to be by 0.3 fraction of the subclass earlier. In order to evaluate the effective temperature from the subclass, we use M giant data, presented in Table 1 of Flower (1975). The appropriate values of T_{eff} are given in the last line of Table 5. Draw a conclusion that the use of the relationships between the band head intensity jumps of titanium oxide α–system and the spectral subclass published by Boyarchuk (1969) allows evaluation of AI CMi effective temperature with an intrinsic error of the mean not worse than 2%, and a systematic error due to spectral resolution uncertainty of about 1%. It should be noted that for some relationships in Fig. 3 from Boyarchuk (1969) the band identification became outdated. For instance, the bands λ 6159 and λ 6215, identified as transitions (1;4) and (2;5) of the α–system, respectively, are identified in Table 5 of the paper by Phillips (1969) as belonging to different branches of (0;0) transition of a new γ'–system of TiO. A review of investigations of six titanium oxide electron transition systems is given by Panchuk (1978).

5.2. T_{eff} estimation from vibrational temperatures T_{vib}

Let us estimate the temperature of the region where the titanium oxide spectrum is formed on the assumption that the vibrational level population is a Boltzmann one. If the vibrational bands belong to the same electron system, then the Boltzmann temperature T_{vib} can be derived from the ratio of residual intensities $i = (I_{\lambda+}/I_{\lambda-})$ of the two vibrational bands:

$$i_1/i_2 = (\nu_1 q_1/\nu_2 q_2)\exp[(E_1 - E_2)/kT_{vib}], \qquad (1)$$

where ν is the frequency of the band head, q is a Frank-Condon factor, the energy of the lower vibrational level $E = hc[w_e(\nu'' + 1/2) + w_e x_e(\nu'' + 1/2)^2]$, ν'' is a vibrational quantum number of the lower level, $w_e x_e$ is an anharmonic factor. Relationship (1) is derived through the substitution of $R_e^2(r_{\nu'\nu''})q_{\nu'\nu''}$ ratio by the ratio of factors $q_{\nu'\nu''}$. The assumption about the weak dependence of the square of the electron transition momentum $R_e^2(r_{\nu'\nu''})$ on the internuclear distance $r_{\nu'\nu''}$ is valid for parallel types of transitions, when the projection of the electron orbital momentum on the internuclear axis is unchanged. It is this category of transitions that the α–system belongs to. Table 6 presents the results of Boltzmann vibrational temperature estimations. Molecular constants, which are needed for calculations, are taken from McCallum et al. (1970). From Table 6 it follows that the accuracy of determination of vibrational temperature for the layer in which the titanium oxide spectrum is originated is by nearly an order of magnitude lower (18%) than that of the method using Boyarchuk (1969) data and Flower (1975) calibrations. Note that in the paper by Morozova and Panchuk (1978) the root mean square error of vibrational temperature determination for Mira-type star atmospheres from all pairs of 10 TiO bands measured on the same photographic spectrograms is equal to 280 K, i.e. 20% of the measured quantity. The low accuracy of temperature determination from the vibrational spectrum of TiO is chiefly due to the different degree of blocking the photospheric continuum for the parts of spectrum in front of the band heads, which are believed in the method used to be free from molecular absorption (see Fig. 3). Shavrina (1977) studied vibrational temperature obtained from the TiO α–system spectrum as a function of spectral subclass in a range of M2–M6. Using this dependence, we estimate spectral subclass of AI CMi as M2.5, and together with the Flower (1975) calibrations it yields $T_{eff} = 3500$ K.

5.3. Absorbing layer mass estimation made from titanium oxide spectrum

Estimate parameters for the layer of the AI CMi atmosphere, in which the TiO spectrum originates, assuming the temperature and density to have the same values throughout the layer. For this purpose calculate the absorption coefficient per titanium oxide molecule. The band model with just overlapping rotational lines (Panchuk, 1975) was used. Because of the blending of lines of different branches and turns of the branches, this approximation is true for the band heads at any realistic values of microturbulent velocity and rotational temperature. Comprehensive evaluation of applicability of the approximation can be found in the paper by Panchuk (1978). The absorption coefficient for the electron–vibrational band system smoothed over the rotational structure is equal per molecule:

$$\begin{aligned}\alpha_\lambda = 2.689 \cdot 10^{-14}(S_e/\lambda Q) \times \\ \exp(-hcE_{e''}/kT)\exp(-hc\Delta G_0/kT) \times \\ [1 - \exp(-hc/k\lambda T)]\Sigma(q_{\nu'\nu''}/\Delta B_\nu) \times \\ \exp(hcB_{\nu'}B_{\nu''}/kT\Delta B_\nu) \times \\ \exp\{(-hc/kT)[(B_{\nu''}/\lambda\Delta B_\nu) - \\ (\Delta B_{\nu'}/\lambda_{\nu'\nu''}\Delta B_\nu) + G_0(\nu)]\}. \qquad (2)\end{aligned}$$

Here Q is the total statistical sum, the approximations $G_0(\nu) = \omega_0\nu - \omega_e x_e \nu^2$, $\omega_0 = \omega_e - \omega_e x_e$, $\Delta G_0 = 0.5\omega_e - 0.25\omega_e x_e$ are used. Summation of separate band contributions to the absorption coefficient is made taking into account the sign of band degradation. The values of electron transitions S_e for six electron–vibrational systems (triplets α, γ', γ, and

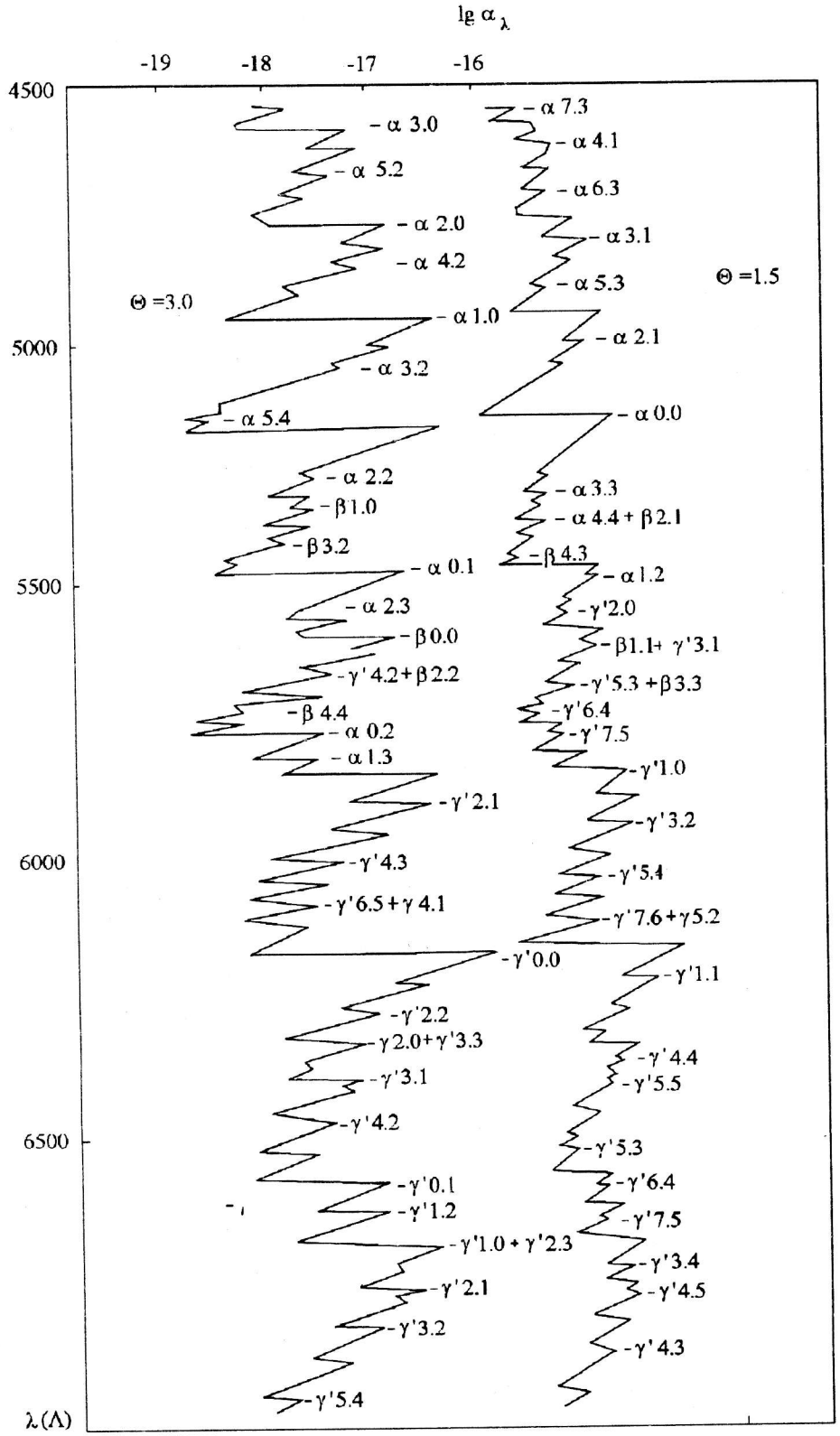

Figure 3: *Absorption coefficient per TiO molecule, calculated under the approximation of overlapping rotational lines for two values of inverse temperature* $\Theta = 5040/\mathrm{T}$. *The identification of electron systems* $(\alpha, \beta, \gamma', \gamma)$ *and vibrational transitions is marked. Values* α_λ *for* $\Theta = 1.5$ *are shifted to the right by two orders.*

Table 5: *Characteristics of the TiO α-system bands in the AI CMi spectrum*

				$\Delta\lambda = 2.4$Å		$\Delta\lambda = 3.6$Å	
	ν', ν''	$q_{\nu',\nu''}$	N	$(I_{\lambda+}/I_{\lambda-})$	Sp	$(I_{\lambda+}/I_{\lambda-})$	Sp
4761	(2;0)	0.172	2	0.49	M2.7	0.49	M2.7
4804	(3;1)	0.230	3	0.63	3.0	0.66	2.6
4955	(1;0)	0.354	6	0.37	2.3	0.42	1.9
5000	(2;1)	0.189	7	0.66	3.4	0.77	2.3
5167	(0;0)	0.394	10	0.29	2.1	0.31	1.9
5240	(1;1)	0.002	11	0.82	2.6	0.86	2.4
5448	(0;1)	0.378	15	0.63	1.3	0.67	1.2
5759	(0;2)	0.171	19	0.74	3.8	0.77	3.4
				Mean	M2.6±0.28		M2.3±0.10
				Mean	T_{eff}(K) 3492.		3516

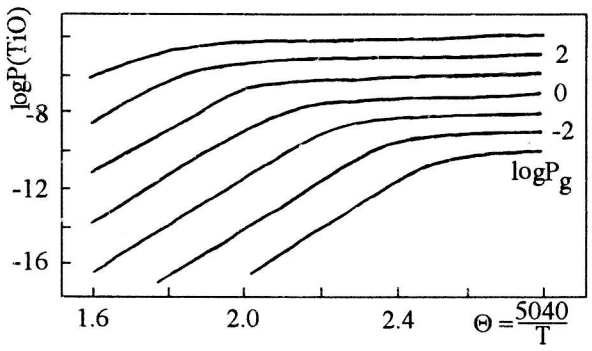

Figure 4: *Partial pressure of titanium oxide as a function of gas pressure* P_g *and inverse temperature* $\Theta = 5040/T$.

Table 6: *Temperatures* T_{vib} *determined from vibrational transitions of TiO α-system.*

λ	$\nu';\nu''$	λ	$\nu';\nu''$	T_{vib}	λ	$\nu';\nu''$	λ	$\nu';\nu''$	T_{vib}
4761	(2;0)	5000	(2;1)	4815	4955	(1;0)	5759	(0;2)	1561
4761	(2;0)	5759	(0;2)	4030	5000	(2;1)	5759	(0;2)	3479
4804	(3;1)	5759	(0;2)	1946	5167	(0;0)	5448	(0;1)	1401
4955	(1;0)	4804	(3;1)	1307	5167	(0;0)	5759	(0;2)	1303
4955	(1;0)	5448	(0;1)	2172	5448	(0;1)	5759	(0;2)	1219
Mean									2323±413

Table 7: *To the estimate of mass of absorbing layer which form AI CMi molecular spectrum in the "cool phase"*

Sp	Band	$\alpha_\lambda(\theta = 2)$	log n(TiO)	log N	log m_o
M2	α(3;1)	-17.0	16.0	23.5	-0.1
M3	α(3;0)	-17.3	16.3	23.8	+0.2
M3	β(0;0)	-16.9	15.9	23.4	-0.2
M3	γ'(1;0)	-16.5	15.5	23.0	-0.6

singlets β, δ and ϕ) are taken from the papers by Fairbairn et al. (1974) and Tsuji (1976). Examples of calculations for two temperature values in the spectrum region corresponding to the fourth AI CMi echelle spectrogram are shown in Fig. 3. Next for a grid of gas pressure P_g and temperature values we solved numerically ionization and dissociative equilibrium equations for a mixture of 36 chemical elements, bearing in mind that 250 molecules will be formed. The method of simultaneous solving ionization and dissociation equations is reported by Panchuk (1975).

The dissociation coustants from Tsuji (1973) were used. In Fig. 4 are displayed the results of TiO molecule partial pressure calculations for solar chemical composition. Knowing the absorption coefficient $\alpha_\lambda(Q)$ per TiO molecule and the relationship between p(TiO) and P_g and Θ, we next attempt to evaluate the matter mass m_0 of an atmosphere column with a base of 1 cm^2, which is needed for band heads with specified intensity to be formed. An important condition should be noted here, which simplifies the evaluation. In the domain of temperatures $\Theta_0 > 2.1$ and pressure $\log P_g > 1$, which are characteristic for the outer layers of M stars, a partial pressure of titanium oxide molecules varies proportionally with a gas pressure. Explain this phenomenon qualitatively. The point is that in a mixture, for which oxygen atoms predominate over carbon ones, all the carbon is bound in CO molecules, while the remaining atoms of the free oxygen is far in excess (by 2–3 orders of magnitude) than the number of metal atoms capable of oxidizing. With temperature drop below Θ_0 further increase in the number of TiO molecules is impossible because practically all the Ti atoms are already bound in TiO molecules. It should be particularly emphasized that with decreasing metallicity, which is accompanied by a decrease in the total number of Ti atoms, the partial pressure P(TiO) saturation effect occurs at higher temperatures, i.e. at lower Θ values. This is due to the fact that most of the TiO atoms are bound into molecules earlier (i.e. at higher temperatures) because the rate of decrease in the content of oxygen atoms in the halo stars is lower than that in metallicity. Therefore having an estimate of m_0 for solar chemical composition, the column mass can be readily recalculated to a metal defficient chemical composition by adding to m_0 the [Ti/H] quantity reversed in sign.

Now estimate the number of molecules n(TiO) necessary for the bands to appear in the spectrum, needed for MK classification. To this end we make use of a thin layer model, assuming that the appearance of the band in the spectrum is caused by the band head residual intensity equal to 0.9 of the continuum level. Table 7 presents the spectral subclass and the TiO bands, the occurence of which is a criterion of spectral classification (Keenan, 1966; Keenan et al., 1974). Further there indicated the values of absorption coefficient per molecule α_λ, derived from formula above given, next follows the number of TiO molecules, total number of particles N, and the mass m_0 of the absorbing layer column with the 1 cm^2 base, calculated for solar chemical composition. Solution of the set of equations of state shows that at $\Theta = 2$ molecular hydrogen is produced in large quantities, beginning from $\log P_g = 3$, so to estimate m_0 we have adopted its average molecular weight in the atmosphere to be $\mu = 1.6$. Thus, when MK classification is applied, the mass of the absorption layer column of 1 cm^2 in base must be $m_0 = 0.79$ g to produce spectral details of spectral class M2, and 0.63, on the average for M3. For spectral class M2.5 with solar chemical composition $m_0 = 0.71$ g.

Determine now the m_0/M ratio, where M is the atmosphere mass in the column with the 1 cm^2 base above the layer with the temperature equal to T_{eff}. To determine M, integrate mass distributions for five atmosphere models. Besides, determine the temperature of the layer, above which the absorbing layer of mass m_0 is situated. The above estimate of $T_{eff} = 3500$ K for AI CMi is beyond the available parameters of the grids of models, thus in Table 8 we present the results for the models selected with the aim of extrapolation. The models of Tsuji (1976) enable us to estimate with assurance for $T_{eff} = 3500$ K the ratio $T_0/T_{eff} = 0.69$, where T_0 is the temperature of the layer responsible for the TiO spectrum. The models of Bell et al. (1976) do not give fine structure break-down of the outer atmosphere, and the first layer contains a mass exceeding m_0. Therefore for these models the T_0/T_{eff} estimate is less reliable. From Fig 3 it follows that the absorption coefficient per molecule α_λ near the band heads with a low ν is little responsive to temperature. Thus the T_0 estimate presented in Table 8 may be thought to be dependent only on T_{eff} determined above by the two different methods.

As was mentioned, the atmosphere mass needed for the observed band heads to originate is about 7 g, with metallicity of -1.0 dex. This will increase m_0/M by an order of magnitude, while the T_0/T_{eff} values will decrease by a few percent. The obtained values of m_0/M indicated that the homogeneous layer approximation is justified. It should be emphasized that such a small fraction of atmosphere responsible for titanium oxide spectrum formation may turn out to be extremely sensitive to all kinds of disturbances, which will eventually result in essential variations of the visible light of the object, caused by the strong blanketing effect of TiO molecules in the visible region.

Table 8: *To the estimate of mass of the atmosphere layer forming TiO spectrum*

T_{eff}/log g	m_o/M	T_o	T_o/T_{eff}	References
4000/0.0	0.0031	2660	0.66	Tsuji, 1976
3600/0.0	0.0021	2494	0.69	Tsuji, 1976
3600/-0.5	0.0014	2498	0.69	Tsuji, 1976
3750/1.5	0.0045	<2363	<0.63	Bell et al., 1976
4000/0.0	0.0029	<2600	<0.65	Bell et al., 1976

Table 9: *The estimate of T_{eff} of the atmosphere model in the "cool" phase from the FeI spectrum*

T_{eff}	log g	ξ_t	[A]	$\log\epsilon$(Fe)	S(χ_L)	T_{eff} $\log\epsilon(Fe) = -5.63$	T_{eff} $S(\chi_L) = 0$
4500	0.0	4.0	-1.0	-5.19	-0.117		
4250	0.0	4.0	-1.0	-5.47	-0.029		
4000	0.0	4.0	-1.0	-5.73	0.039		
3500	0.0	4.0	-1.0	-6.28			
						4100	4170
4500	0.0	5.0	-1.0	-5.31	-0.116		
4250	0.0	5.0	-1.0	-5.59	-0.021		
4000	0.0	5.0	-1.0	-5.86	0.046		
3500	0.0	5.0	-1.0	-6.40			
						4100	4170

5.4. Estimation of AI CMi model parameters in the "cool" phase from the atomic spectrum

Proceed to estimating atmosphere parameters from the atomic spectrum of AI CMi in the "cool" phase (11.12.95). Assume that the star metallicity in the "hot" and "cool" phases is equal. In Table 9 are given the results of calculations of iron abundance, using the equivalent widths from Table 2, for three models with T_{eff} of 4500, 4250 and 4000 K and two values of microturbulent velocities 4 and 5 km/s. Extrapolation of $\log\varepsilon$ (Fe) to values, corresponding to effective temperature of 3500 K evaluated from the TiO spectrum, gives an iron abundance which is, on average, by 0.7 dex lower than that obtained from the "hot" phase spectrum. A dependence S(χ_L) of $\log\varepsilon$ (Fe) on excitation potential of the lower level χ_L of the used line changes its inclination sign, which is evidence of higher T_{eff}. At low temperatures most of the iron exists in the form of neutral atoms, that is why luminosity variations do not permit $T_{eff} = 3500$ K to be related to the metallicity obtained from the "hot" phase. In Table 9 are presented T_{eff} values derived for the two values of microturbulent velocity from the condition of equality of the "hot" and "cool" phases metallicity $\log\varepsilon$ (Fe) = −5.63 and Boltzmann "equilibrium" for neutral iron atomic levels S(χ_L) = 0. Therefore in further calculations of AI CMi chemical composition from the spectrum in the "cool" phase we used models with $T_{eff} = 4100$ K, $\xi_t = 4$ km/s, [Fe/H]=-1.0, log g being varied. Within the used grid of models log g = −0.75 turns out to be the most reasonable value, for this set of parameters we performed determination of AI CMi chemical composition in the "cool" phase (see Table 4).

Table 10: *Relationship of metal partial pressure jumps* $\Delta\log p(X)$ *while [O/C] ratio being varied with dissociation energy of monooxides* $D_o(XO)$.

X	$D_o(XO)$	$\Delta\log p(X)$	$\Delta\log\epsilon(X)$
B	184	2.0	
Ti	156	0.5	-0.16
V	147		-0.10
Y	169	0.7	-0.23
Zr	181	1.9	-0.35
La	191	1.4	+0.31
Ce	185	2.5	

5.5. Characteristics of the layers that form atomic and molecular spectra

Let us consider why T_{eff} values obtained for the "cool" phase from TiO and neutral iron spectra (3500 and 4100 K, respectively) are so different. At first compare effective depths at which the considered spectral features originate. For each of the neutral iron lines we calculated m_1, the mass of the atmosphere column with the 1 cm^2 base above the effective (i.e. weighted mean by flux in the line) level of the given line formation. For lines having equivalent widths from 27 to 238 mÅ m_1 – value ranges from 2239 to 155 g, the mean value of m_1 obtained over 70 FeI lines of the "cool" phase spectrum is 759 g. Therefore, the neutral iron spectrum is formed effectively in the 9–22-th layers of the model with T_{eff} = 4100 K, log g=-0.75, [A]=-1. As demonstrated above, the mass of a similar atmospheric column needed for TiO spectrum formation does not exceed 7 g, i.e. the whole titanium oxide spectrum must be formed even in the first layer (its mass is 14 g) of the indicated model. Come to the conclusion that the regions of molecular and atomic spectrum formation are essentially spaced apart in atmosphere depth and, which is as important, are basically different in mass of the contained matter. The temperature of the first layer of the model having a mass sufficient for the TiO spectrum to be formed, is equal to 2747 K, but this value does not agree with that obtained from the TiO spectrum. So, from Table 8 it follows that the temperature of the layer, in which TiO α–system spectrum is formed, is equal to 2500 K, when T_{eff} = 3600 K. Thus, in order to satisfy the condition of maintaining the metallicity and appearance of molecular bands, we must adopt the model with T_{eff} = 4100 K, log g=-0.75, [A]=-1, and an outer layer temperature by 9 % lower than the self-consistent temperature of the model.

6. Discussion

Let us examine the results of AI CMi chemical composition determination. First of all we have compared the values of standard deviation σ of AI CMi chemical composition determination, presented in Table 4 from Luck and Bond (1989) with the errors of average chemical composition determination, taken from Table 4 of our work. We will arrive at a conclusion, that inherent accuracy of chemical composition determination is the same in both papers. Now compare abundances, normalizing on the iron abundance, which is the same in both papers. The average excess of α–process element abundances (Na, Mg, Al, Si) from our spectra is [α/Fe] = +0.33, whereas Luck and Bond (1989) report for Na, Al and Si [α/Fe] = +0.39. The average defficiency of s–process element abundances (La, Ce, Pr, Nd) from our spectra is [s/Fe] = −0.35, while Luck and Bond (1989) report for La, Ce, and Nd [s/Fe]=-0.46. Out of 20 chemical elements, the abundances of which are studied by Luck and Bond (1989), and 26 elements from Table 4 of our work 18 elements are common. The average difference in abundances of common elements is -0.02 dex. Sc, Ti, Y, Ce showed abundance differences of more than 0.4 dex. The O/Fe ratio determined from the forbidden oxygen line is by 0.87 dex higher than that of solar atmosphere. We come to a conclusion that from 1981 to 1995 abundances of elements heavier than oxygen remained the same in the AI CMi atmosphere, i.e. no transfer of matter processed in the inner layers of the star to the star's atmosphere is observed.

Now consider possible causes of difference in the temperature of the outer atmosphere layers during the "cool" phase, which was estimated from the atomic and molecular spectra. In the frames of one–dimensional model a mechanism to account for the molecular spectra formation in the outer layer should be suggested, which would not cause essential changes in the parameters of the layers responsible for the atomic spectrum. There are the three approaches.

Luck and Bond (1989) did not determine the oxygen abundance in the AI CMi atmosphere. Therefore it can be suggested at first that oxygen–to–carbon ratio [O/C] in the atmosphere increased. Illustrate this effect quantitatively. In Fig. 5 are presented the results of the solution of a set of dissociation equations for a collection of $\log\varepsilon$ (C) values. It is seen that with increasing [O/C] the abundance of molecules containing oxygen increases, while the abundance of free atoms of metals decreases. The degree of molecular dissociation in atmospheres of carbon stars is lower than that of M-stars because the energies of dissociation of carbides and dicarbides are lower than the energies of oxides dissociation. If the carbon abundance is close to the oxygen, partial pressures of metals sharply increase by different values of $\Delta \log p$. In Table 10 are presented $\Delta \lg p$ from Fig. 5 and dissociation energies D_0 (kkal/mol) taken from Krasnov et al. (1968) of basic compounds of these metals — monooxides. The values of $\Delta \log p$ and D_0 from Table 10 correlate, which confirms the suggestion that the main role in control of partial pressures of free atoms, when the pressures pass the value [O/C]=1, is played by monooxides. The Kurucz algorithms for determination of chemical composition we are using in our calculations do not take account of the diversity of molecules that we allow for when solving the dissociation equations (250 kinds of molecules). Therefore, if [O/C] increases when passing to the "cool" phase, the effect of correlation between $\Delta \log p$ and D_0 must show up in underestimation of $\log\varepsilon$ (x) values determined for the "cool" phase. Since in the AI CMi "cool" phase the spectrum features of M–star are observed, i.e. [O/C] does not go over unity,

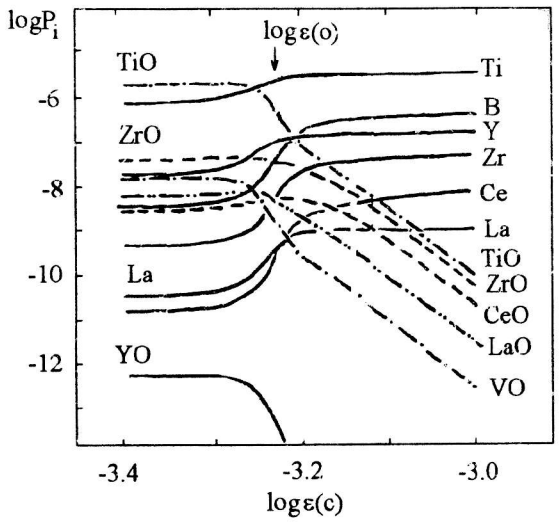

Figure 5: *The relationship of partial pressures* P_i *of the selected atoms and molecules as a function of carbon abundance* $\log\varepsilon(C)$. *The total gas pressure, temperature and oxygen abundance are constant* ($\log P_g = 2; \Theta = 2; \log\varepsilon(0) = -3.23$).

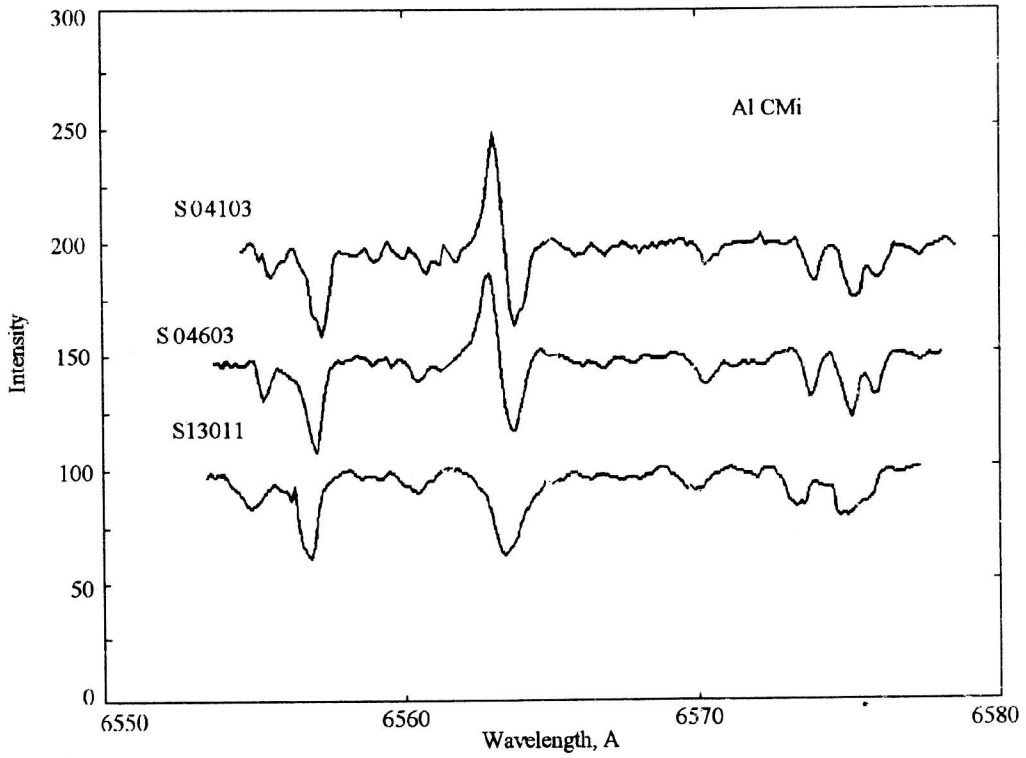

Figure 6: *Fragments of the AI CMi spectra near* H_α.

then an expected error of $\Delta\log\varepsilon(x)$ must be less than $\Delta\log p$. In the last column of Table 10 $\Delta\log\varepsilon(x)$ values differences obtained for the "hot" and "cool" phases are presented. In most cases these differences do not exceed determination errors of the corresponding $\log\varepsilon(x)$, therefore, despite the sign of the effect for four elements out of five measured is the expected one, we consider the suggestion that [O/C] increases in the AI CMi atmosphere when going to the "cool" phase to be not verified yet.

Second, it may be supposed that in the outermost atmosphere layers of cool stars the condition of dis-

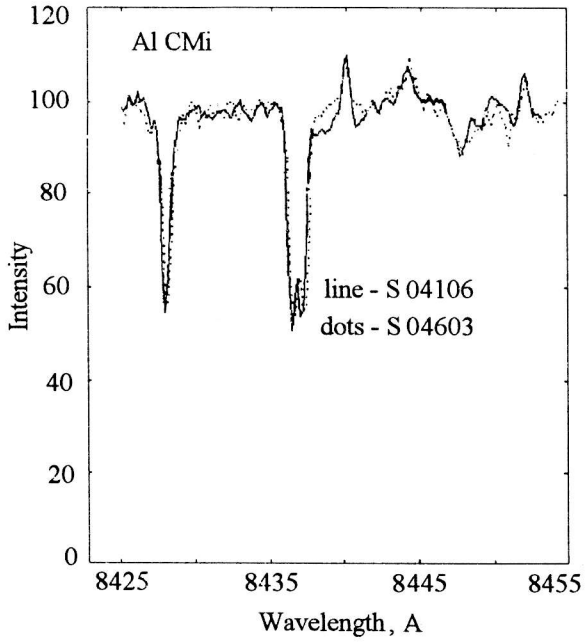

Figure 7: *Fragments of the AI CMi spectra near* P_{10}.

sociative equilibrium is not satisfied. For instance, it was revealed that conditions in the atmosphere of the Mira–type star R Leo for hydroxyl molecules falls off from thermochemical equilibrium (Panchuk, Tsymbal, 1982). It should be stressed that under the dissociative equilibrium condition concentration of hydroxyle molecules is on average by two orders of magnitude higher than that of titanium oxide molecules, so, even at minor departures from dissociative equilibrium for OH, TiO is likely to fall off from equilibrium too. The low mass of the layer responsible for the TiO spectrum makes it highly responsive to various disturbances. It should be noted here that in AI CMi spectra there are some features which can be interpreted as evidence of departure from thermodynamic equilibrium in the atmosphere outer layers. Fig. 6 presents the spectrum fragments of the orders that contain the H_α line, while Fig. 7 presents a spectrum portion with the Paschen series hydrogen line. It follows from the figures that the departure from thermodynamic equilibrium in the AI CMi atmosphere varies.

Third, the most simple explanation for the spectrum of TiO to appear at $T_{eff} = 4100$ K is also possible: the outer layer temperature in the model used is overestimated by 200–300 K because of the underestimated blanketing effect.

When beyond the scope of the classical approximation — one-dimensional model atmosphere — and recalling the flux inhomogeneities over the disk of the star to have been detected in the brightest cool stars, we come to a fourth explanation of the TiO bands appearance phenomenon. Assume that the flux inhomogeneities are caused by surface temperature inhomogeneities, and their amplitude is about 10 %. In the "hot" phase these inhomogeneities are characterized by minimum temperatures insufficient for the TiO spectrum to be formed, and therefore only atomic and ion lines are observable. In the "cool" phase with the same scatter (10 %) of surface temperature values "cool" regions form absorption spectrum in TiO bands with several first vibrational quantum numbers. It is selfevident that in such a model the areas of cool and hot region surfaces must be of the same order of magnitude.

The work was accomplished under GSTP "Astronomy" financial support. The authors are very grateful to Prof. B. Gustafsson for permission to use unpublished model atmospheres.

References

Boyarchuk M.E.: 1969, Izv.Crim.Astrofiz. Obs., **39**, 114.
Bell R.A., Eriksson K., Gustafsson B., Nordlund A.: 1976, Astron. Astrophys. Suppl. Ser., **23**, 37.
Eggen O.J., 1983, Astron. J., **88**, 386.
Fairbairn A.R., Wolnik S.J., Berthel R.O.: 1974, Astrophys. J., **193**, 273.
Flower P.J.: 1975. Astron. Astrophys., **41**, 391.
Galazutdinov G.A.: 1992, Preprint of SAO RAS, **92**.
Grevesse N.: 1993, The paper reported at d'Evry Schatzman Colloquium "Physical Processes in Astrophysics" held at Paris Observ.
Kamenszikov V.A., Plastinin Yu.A., Nikolaev V.M., Novitskij L.A.: 1971, Radiation characteristic of gases at high temperatures. "Mashinostroenie", Moscow, 1971.
Keenan P.C.: 1966, Astrophys. J. Suppl. Ser., **13**, 333.
Keenan P.C., Garrison R.F., Deutsch A.J.: 1974, Astrophys. J. Suppl. Ser., **28**, 271.
Kholopov P.N., Samus' N.N., Frolov M.S., et al.: 1985, General Catalogue of Variable Stars (Fourth edition), Moscow.
Klochkova V.G.: 1995, Mon. Not. R. Astron. Soc., **272**, 710.
Klochkova V.G., Panchuk V.E., Chentsov E.L.: 1996, Astron. Astrophys., accepted.
Krasnov K.S., Timoshinin V.S., Danilova T.G., Khandogko S.V.: 1968, Molecular constants of nonorganic combinations, "Khimiya", Leningrad.
Kukarkin B.V., Kholopov P.N., Efremov Yu.N., et al.: 1969, General Catalogue of Variable Stars (Third edition), Moscow.
Kurucz R.L.: 1975, Smithsonian Astrophys. Observ. Special Report No.309.
Luck R.E.: 1991, Astrophys. J., **75**, 759.
Luck R.E., Bond H.E.: 1989, Astrophys. J., **342**, 476.
McCallum J.C., Jarmain W.R., Nicholls R.W.: 1970, Spectroscopic Report No. 1, York Univ. CRESS.
McCallum J.C., Nicholls R.W.: 1971, Spectroscopic Report No. 2, York Univ. CRESS.
MacConnel D.J., Bidelmann W.P.: 1976, Astron. J., **81**, 225.

einel A.B., Aveni A.F., Stockton M.W.: 1969, Catalog of emission lines in astrophysical objects. Second edition. Optical Sciences Center and Steward Observ., Univ. of Arizona, Tucson.
lorozova S.M., Panchuk V.E.: 1978, Soobshch. Spets. Astrofiz. Obs., **22**, 27.
anchuk V.E.: 1974, Astrometriya and Astrofiz.. **22**, 37.
anchuk V.E.: 1975, Astrometriya and Astrofiz., **25**, 20.
anchuk V.E.: 1978, Soobshch.Spets.Astrofiz.Obs., **22**, 5.
anchuk V.E., Tsymbal V.V.: 1992, Astrofiz.Issled. (Izv.SAO), **16**, 12.
anchuk V.E , Klochkova V.G., Galazutdinov G.A., et al.: 1993, Pis'ma Astron. Zh., **19**, 1061.
Phillips J.G.: 1969, Astrophys. J., **157**, 449.
Shavrina A.V : 1977, Astrometriya and Astrofiz., **32**, 29.
Thevenin F.: 1989, Astron. Astrophys. Suppl. Ser., **77**, 137.
Thevenin F.: 1990, Astron. Astrophys. Suppl. Ser., **82**, 179.
Tsuji T.: 1976, Publ. Astron.Soc.Japan, **28**, 543.
Tsuji T., 1973, Astron. Astrophys., **23**, 411.
Zacz L., Klochkova V.G., Panchuk V.E.: 1995, Mon. Not. R. Astron. Soc., **275**, 764.
Zacz L., Klochkova V.G., Panchuk V.E.: 1996, Mon. Not. R. Astron. Soc., accepted.

Table 2: *Atomic data, measured equivalent widths W of lines in the spectra of AI CMi*

Element	λ, Å	EP	log gf	W		
				S04103	S04603	S13011
Li I	6707.766	0.000	6.180E-01	5	5	
[OI]	6300.304	0.000	1.770E-10		152	245
O I	7771.944	9.150	2.138E+00	149	144	
O I	7774.167	9.150	1.549E+00	146	127	
O I	7775.388	9.150	9.333E-01	112	121	
Na I	5682.647	2.100	1.950E-01		116	153
Na I	5688.217	2.100	3.981E-01	138		180
Na I	6154.230	2.100	2.692E-02	35	22	78
Na I	6160.753	2.100	5.370E-02	42		
Mg I	5711.095	4.340	2.075E-02	129	110	168
Mg I	6318.708	5.108	1.072E-02	50	28	
Mg I	6319.242	5.110	6.310E-03	12		
Mg I	8473.68	5.930	0.980E-03		2	
Mg I	8712.701	5.930	8.128E-02	47		
Mg I	8717.833	5.930	1.380E-01	76		
Al I	5557.070	3.140	1.122E-02	10		
Al I	6696.032	3.140	4.786E-02	22	30	
Al I	6698.669	3.140	2.399E-02	19		
Al I	7084.656	4.020	1.778E-01	14		
Al I	8773.91	4.020	8.710E-01		52	
Si I	5645.618	4.930	7.244E-03	44	18	
Si I	5665.563	4.920	9.120E-03	42	43	
Si I	5666.687	5.610	1.622E-02	16		
Si I	5684.493	4.950	2.239E-02	109		
Si I	5690.433	4.930	1.349E-02			82
Si I	5701.109	4.930	8.913E-03	47		
Si I	5708.406	4.950	3.388E-02	92	98	142
Si I	5753.646	5.610	5.023E-02	32		
Si I	5772.149	5.080	1.778E-02	39	53	
Si I	5793.079	4.930	8.710E-03	53	52	
Si I	5797.865	4.950	8.913E-03	86		
Si I	5873.770	4.930	9.226E-04	18	16	
Si I	5948.548	5.080	5.888E-02	83	78	
Si I	6087.790	5.870	1.932E-02	14		
Si I	6091.920	5.870	3.945E-02	11		
Si I	6125.027	5.610	3.069E-02			34
Si I	6142.492	5.620	2.884E-02	27	12	
Si I	6145.020	5.610	3.319E-02	26	19	24
Si I	6155.142	5.620	1.081E-01	75	63	
Si I	6237.328	5.610	7.278E-02	34		
Si I	6243.82	5.620	4.570E-02	20	18	
Si I	6244.13	5.620	4.365E-02	13		
Si I	6414.987	5.870	6.998E-02	21	51	
Si I	6741.629	5.980	1.738E-02	35		
Si I	6976.504	5.950	6.761E-02	55	27	

Element	λ, Å	EP	log gf	W		
				S04103	S04603	S13011
Si I	7003.574	5.960	2.371E-01	64		
Si I	7034.910	5.870	1.318E-01	32		
Si I	7405.790	5.610	2.871E-01		119	
Si I	7415.958	5.610	3.491E-01		132	
Si I	8556.797	5.870	6.383E-01		112	
Si I	8742.466	5.870	3.090E-01		108	
Si I	8752.02	5.870	4.268E-01		137	
Si II	6347.094	8.120	1.820E+00	72		
S I	8693.150	7.870	3.802E-02	8		
S I	8693.958	7.870	2.754E-01	33		
S I	8694.641	7.870	1.072E+00	16		
Ca I	5349.469	2.710	4.898E-01			196
Ca I	5581.979	2.520	2.786E-01	124	119	113
Ca I	5588.764	2.520	2.280E+00	212		244
Ca I	5590.126	2.520	2.685E-01	71		91
Ca I	5594.471	2.520	1.250E+00	193	190	265
Ca I	5598.491	2.520	8.185E-01	192		
Ca I	5601.286	2.520	2.999E-01	72		
Ca I	6102.727	1.880	1.611E-01	243	221	
Ca I	6161.295	2.520	5.420E-02	48	57	
Ca I	6162.180	1.900	8.128E-01	260	272	
Ca I	6166.440	2.520	7.211E-02	28		
Ca I	6169.044	2.520	1.596E-01	81		
Ca I	6169.564	2.520	3.327E-01	96		
Ca I	6439.083	2.520	2.455E+00		236	
Ca I	6449.810	2.521	3.148E-01		241	
Ca I	6471.668	2.520	2.061E-01	93	124	220
Ca I	6493.788	2.520	7.780E-01	169	166	164
Ca I	6499.654	2.520	1.521E-01	91		
Ca I	6572.795	0.000	4.898E-05	91		214
Ca I	7148.150	2.710	1.371E+00	135		
Ca I	7202.208	2.710	5.470E-01	128		
Sc II	5239.810	1.455	1.698E-01			243
Sc II	5318.370	1.357	9.120E-03			81
Sc II	5357.190	1.507	6.166E-03			127
Sc II	5552.237	1.450	5.370E-03			32
Sc II	5640.988	1.500	9.772E-02	120		193
Sc II	5667.153	1.500	6.310E-02	69		230
Sc II	5669.039	1.500	8.128E-02	86	67	
Sc II	5684.31	1.510	9.772E-02	92		
Sc II	6245.620	1.510	1.175E-01	60	79	
Sc II	6279.740	1.500	6.918E-02	69		
Sc II	6320.844	1.500	1.950E-02	13	25	
Sc II	6604.580	1.357	3.311E-02	44	38	
Ti I	5045.400	0.848	1.143E-02			198
Ti I	5644.14	2.270	1.000E+00	83	69	
Ti I	5648.570	2.495	6.252E-01	21		
Ti I	5716.450	2.297	2.270E-01	44		

Element	λ, Å	EP	log gf	W		
				S04103	S04603	S13011
Ti I	5720.450	2.292	1.432E-01	23		
Ti I	5774.040	3.305	3.436E+00	23	46	
Ti I	5839.76	1.460	4.365E-03	10		
Ti I	5866.450	1.067	1.644E-01	230		
Ti I	5880.310	1.053	1.026E-02	82	85	
Ti I	5903.320	1.067	8.147E-03			138
Ti I	5918.550	1.067	3.945E-02	119	123	
Ti I	5922.110	1.046	3.890E-02	144	149	
Ti I	5937.810	1.067	1.466E-02	51	65	
Ti I	5940.65	0.050	9.332E-04	86	80	
Ti I	5944.68	0.000	1.622E-04	89		
Ti I	5953.160	1.887	5.333E-01	101	111	
Ti I	5965.830	1.879	4.436E-01	84	90	
Ti I	5999.69	2.240	1.660E-01	31	39	
Ti I	6031.71	0.050	1.778E-04	62	51	
Ti I	6064.630	1.046	1.294E-02	105		197
Ti I	6091.180	2.267	4.295E-01	54	49	86
Ti I	6092.810	1.887	4.753E-02		22	
Ti I	6126.220	1.067	4.276E-02			200
Ti I	6146.23	1.870	3.020E-02	15		
Ti I	6261.100	1.430	3.776E-01	189		
Ti I	6303.750	1.443	3.090E-02	50	53	114
Ti I	6312.240	1.460	3.192E-02	46	52	104
Ti I	6325.16	0.020	3.548E-04	122		
Ti I	6336.100	1.443	2.056E-02	38	39	
Ti I	6366.35	1.460	1.820E-02			162
Ti I	6497.68	1.440	1.047E-02	77		
Ti I	6508.15	1.430	2.239E-03	24		
Ti I	6554.230	1.443	6.887E-02	88		165
Ti I	6599.110	0.900	9.354E-03	98	102	
Ti I	6666.550	1.460	2.793E-02	18		
Ti I	6743.120	0.900	2.667E-02	80		
Ti I	7138.910	1.443	2.924E-02	55		
Ti I	7188.550	1.430	1.977E-02	66	35	
Ti I	7357.740	1.443	8.590E-02	125		
Ti II	6559.57	2.050	5.012E-03	56		
Ti II	6606.970	2.061	1.622E-03	15	32	
V I	5604.940	1.043	5.248E-02	16	23	
V I	5668.360	1.081	9.333E-02	58	54	
V I	5670.850	1.081	3.802E-01		91	
V I	5703.590	1.051	6.152E-01	78	145	214
V I	5727.050	1.081	9.727E-01	114	176	
V I	5727.650	1.051	1.349E-01	47	57	
V I	5737.060	1.064	1.820E-01	62	60	
V I	6039.730	1.064	2.239E-01	51	54	
V I	6058.090	1.043	4.227E-02	28	24	85
V I	6081.440	1.051	2.636E-01	71	67	133
V I	6090.210	1.081	8.670E-01	116	106	

Element	λ, Å	EP	log gf	W		
				S04103	S04603	S13011
V I	6111.650	1.043	1.928E-01	48		
V I	6119.530	1.064	4.786E-01	94	100	
V I	6135.37	1.050	1.778E-01	42	63	
V I	6150.160	0.301	1.660E-02	64	57	
V I	6199.190	0.287	5.012E-02	56		
V I	6213.870	0.301	8.913E-03		44	
V I	6216.370	0.275	5.129E-02	90	63	
V I	6224.510	0.287	9.772E-03	51	72	
V I	6251.820	0.287	4.571E-02	91	127	
V I	6266.320	0.275	5.129E-03	26	30	
V I	6274.650	0.267	2.138E-02	29	64	
V I	6531.410	1.218	1.445E-01	22		
V II	5819.930	2.522	1.995E-02	5		
V II	5928.888	2.522	2.570E-02	30		
V II	6028.27	2.490	1.047E-02	9	8	
V II	6029.00	2.560	1.148E-02	3	4	
Cr I	5574.38	4.450	3.548E-01	8		
Cr I	5664.32	3.830	1.259E-01	8		
Cr I	5702.300	3.449	2.153E-01	20		
Cr I	5712.77	3.010	5.888E-02	23		
Cr I	5719.820	3.013	2.188E-02	49		
Cr I	5729.20	3.840	7.079E-02	10		
Cr I	5781.75	3.320	1.412E-01	11	14	
Cr I	5783.110	3.323	3.162E-01	4		
Cr I	5783.890	3.322	5.070E-01	18		
Cr I	5787.970	3.322	8.260E-01	51	28	
Cr I	5788.39	3.010	2.239E-02	26		
Cr I	5825.81	0.970	4.169E-05	8		
Cr I	6330.130	0.941	1.202E-03	46	49	
Cr I	6362.87	0.940	8.318E-04	23		
Cr I	6501.20	0.980	2.188E-04	5	9	
Cr I	6529.18	3.890	4.898E-02	7		
Cr I	6680.15	4.160	3.020E-01	17		
Cr I	6789.15	3.840	6.761E-02	10		
Cr I	6978.460	3.464	1.387E+00	43		
Cr I	6979.810	3.464	3.890E-01	24	36	
Cr I	7400.220	2.900	7.745E-01		87	
Mn I	5377.63	3.840	4.074E-01			40
Mn I	5413.68	3.860	1.349E-01			200
Mn I	6013.480	3.072	5.610E-01	58	60	
Mn I	6016.64	3.070	5.754E-01	56	69	
Mn I	6021.790	3.075	1.081E+00	78	81	
Fe I	5027.13	4.150	5.623E-02			232
Fe I	5029.620	3.415	8.913E-03			136
Fe I	5044.210	2.851	7.079E-03			237
Fe I	5067.150	4.220	1.072E-01			172
Fe I	5074.750	4.220	6.310E-01			250
Fe I	5088.160	4.154	1.660E-02			89

Element	λ, Å	EP	log gf	W		
				S04103	S04603	S13011
Fe I	5090.780	4.256	3.981E-01		173	
Fe I	5143.730	2.198	1.622E-04		114	
Fe I	5217.39	3.210	1.000E-01			236
Fe I	5223.190	3.635	4.074E-03			93
Fe I	5228.410	4.220	5.129E-02			108
Fe I	5231.39	3.570	9.120E-04			15
Fe I	5236.190	4.186	1.905E-02			33
Fe I	5242.490	3.634	1.445E-01			147
Fe I	5243.780	4.256	7.079E-02			67
Fe I	5253.030	2.279	1.148E-04			120
Fe I	5253.460	3.283	2.138E-02			173
Fe I	5288.530	3.695	2.138E-02			91
Fe I	5293.970	4.143	1.349E-02			72
Fe I	5315.070	4.371	2.818E-02			68
Fe I	5321.110	4.435	3.631E-02			30
Fe I	5322.040	2.279	9.333E-04			199
Fe I	5329.990	4.076	5.012E-02			81
Fe I	5373.710	4.473	1.380E-01			95
Fe I	5379.570	3.695	3.311E-02			103
Fe I	5386.340	4.154	1.698E-02			34
Fe I	5398.290	4.446	2.138E-01			96
Fe I	5400.500	4.371	6.918E-01			170
Fe I	5543.150	3.695	2.692E-02			97
Fe I	5543.940	4.218	7.244E-02			98
Fe I	5554.890	4.549	3.631E-01			144
Fe I	5557.950	4.473	5.248E-02			63
Fe I	5560.230	4.435	6.457E-02			76
Fe I	5562.71	4.430	4.467E-03			104
Fe I	5563.600	4.191	1.023E-01	82		135
Fe I	5565.71	4.610	5.129E-01	119	94	169
Fe I	5567.400	2.609	1.585E-03	101	130	160
Fe I	5569.620	3.417	2.884E-01	203	201	
Fe I	5572.840	3.397	4.898E-01	207	250	
Fe I	5576.090	3.430	1.000E-01	155	145	233
Fe I	5584.770	3.573	4.786E-03		44	
Fe I	5586.760	3.368	6.166E-01	270	271	
Fe I	5587.580	4.143	1.413E-02	33		
Fe I	5608.980	4.209	3.981E-03		9	
Fe I	5614.28	5.090	4.169E-02	17		
Fe I	5618.650	4.209	4.169E-02	19	43	68
Fe I	5620.530	4.154	1.622E-02	22		71
Fe I	5633.970	4.991	5.370E-01	57		52
Fe I	5635.850	4.256	1.288E-02	44		
Fe I	5636.710	3.640	2.455E-03	48		
Fe I	5638.270	4.220	1.349E-01	77		115
Fe I	5650.010	5.100	1.202E-01	40	16	
Fe I	5650.710	5.086	1.096E-01	35		
Fe I	5652.320	4.261	1.122E-02	28		

Element	λ, Å	EP	log gf	W		
				S04103	S04603	S13011
Fe I	5653.890	4.386	2.291E-02			32
Fe I	5661.360	4.284	9.550E-03	17		
Fe I	5679.020	4.652	1.202E-01	36	37	
Fe I	5686.530	4.549	2.344E-01	48		159
Fe I	5701.540	2.559	6.081E-03	181		
Fe I	5705.480	4.301	2.512E-02		68	
Fe I	5705.990	4.608	2.951E-01	40		
Fe I	5717.850	4.284	7.413E-02	86	32	
Fe I	5720.890	4.549	1.122E-02	23	6	
Fe I	5731.770	4.256	5.012E-02	58	57	
Fe I	5738.220	4.220	4.571E-03	22	10	
Fe I	5741.860	4.256	1.862E-02	14		
Fe I	5752.04	4.550	1.023E-01	31	36	
Fe I	5753.120	4.261	1.738E-01	64	58	
Fe I	5775.09	4.220	5.888E-02	45	79	
Fe I	5778.470	2.588	2.570E-04	28	46	
Fe I	5793.930	4.220	1.995E-02	30	27	
Fe I	5804.060	3.882	5.129E-03	20		
Fe I	5806.730	4.608	8.913E-02	33	27	
Fe I	5809.250	3.884	1.445E-02	53	38	
Fe I	5811.930	4.143	3.715E-03	4		
Fe I	5816.360	4.549	2.089E-01		50	
Fe I	5827.890	3.283	3.890E-04	13		
Fe I	5837.710	4.294	4.571E-03		12	
Fe I	5849.670	3.695	1.023E-03		22	
Fe I	5852.190	4.549	4.677E-02	19		
Fe I	5853.180	1.485	5.248E-06	67	45	
Fe I	5859.61	4.550	2.519E-01	69		
Fe I	5861.110	4.283	3.548E-03	10		
Fe I	5862.36	4.550	4.169E-01	65		
Fe I	5873.210	4.256	7.244E-03	29		
Fe I	5876.270	4.301	2.239E-03		5	
Fe I	5879.490	4.607	7.244E-03	17		
Fe I	5881.280	4.608	1.445E-02	13	9	
Fe I	5883.840	3.960	4.365E-02	49	58	
Fe I	5909.990	3.211	1.660E-03	43	35	102
Fe I	5916.250	2.453	1.014E-03	91	95	137
Fe I	5920.56	3.240	2.042E-03		13	
Fe I	5927.800	4.652	8.128E-02	44		
Fe I	5929.700	4.549	3.890E-02	48		
Fe I	5930.170	4.652	5.888E-01	101	69	
Fe I	5934.660	3.929	6.761E-02	62		
Fe I	5947.50	4.610	8.912E-03		15	
Fe I	5952.750	3.984	3.631E-02	34		
Fe I	5956.700	0.859	2.483E-05	194		
Fe I	5958.34	2.180	4.677E-05	38	33	
Fe I	5963.26	2.220	1.660E-05	13	6	
Fe I	5987.06	4.800	2.570E-01	58	31	

Element	λ, Å	EP	log gf	W		
				S04103	S04603	S13011
Fe I	5997.78	4.610	8.912E-02	28	50	
Fe I	6003.030	3.882	7.586E-02	113	135	
Fe I	6007.96	4.650	1.738E-01	42		
Fe I	6008.56	3.880	1.047E-01	83	147	
Fe I	6015.250	2.223	2.089E-05	16	14	
Fe I	6019.360	3.573	4.365E-04	11	10	
Fe I	6020.170	4.608	5.370E-01	75	86	
Fe I	6024.070	4.549	7.586E-01	98	111	
Fe I	6027.060	4.076	6.166E-02	39		
Fe I	6055.990	4.733	3.467E-01		45	49
Fe I	6065.480	2.609	2.951E-02	191	247	
Fe I	6078.49	4.800	4.169E-01	55	46	50
Fe I	6078.99	4.800	7.586E-02	33		
Fe I	6082.720	2.223	2.673E-04	76	91	116
Fe I	6094.420	4.652	1.148E-02	10		
Fe I	6096.690	3.984	1.175E-02	36	20	73
Fe I	6102.18	4.830	5.495E-01	98		
Fe I	6103.19	4.830	2.239E-01	95		
Fe I	6114.39	3.930	4.074E-04		4	
Fe I	6120.250	0.915	1.122E-06			103
Fe I	6137.690	2.588	3.954E-02	213	292	
Fe I	6151.620	2.176	5.023E-04	123	138	
Fe I	6157.730	4.076	5.495E-02	52	30	
Fe I	6165.370	4.143	2.818E-02	14		
Fe I	6173.340	2.223	1.318E-03	130	160	
Fe I	6180.220	2.728	1.660E-03	86	93	
Fe I	6188.040	3.943	1.905E-02	33	44	
Fe I	6213.430	2.223	2.188E-03	180	206	
Fe I	6215.150	4.186	3.631E-02	64		
Fe I	6219.280	2.198	3.690E-03	154	175	
Fe I	6226.770	3.884	6.026E-03	32	27	
Fe I	6229.230	2.845	1.072E-03	63	30	
Fe I	6230.730	2.559	5.236E-02	220	255	
Fe I	6232.64	3.650	4.677E-02	68		
Fe I	6240.660	2.223	4.169E-04	77	148	
Fe I	6252.550	2.404	2.056E-02		232	
Fe I	6254.260	2.279	3.311E-03	174	223	
Fe I	6256.370	2.453	2.399E-03	133		
Fe I	6265.130	2.176	2.818E-03	161	206	
Fe I	6270.240	2.858	1.950E-03	41	68	
Fe I	6271.290	3.332	1.122E-03	15	13	
Fe I	6290.550	2.588	4.677E-05			38
Fe I	6293.93	4.830	1.906E-02			17
Fe I	6297.800	2.223	1.820E-03	168		232
Fe I	6301.50	3.650	2.570E-01			212
Fe I	6302.49	3.690	6.918E-02			141
Fe I	6311.510	2.832	5.888E-04		41	113
Fe I	6315.810	4.076	1.950E-02	18		58

Element	λ, Å	EP	log gf	W		
				S04103	S04603	S13011
Fe I	6318.02	2.450	1.000E-02	173	189	
Fe I	6322.690	2.588	3.750E-03	112	156	245
Fe I	6330.860	4.733	1.820E-02	15		
Fe I	6335.340	2.198	5.888E-03	200	244	
Fe I	6336.840	3.686	8.913E-02		109	187
Fe I	6344.150	2.433	1.194E-03	90	127	
Fe I	6353.84	0.910	3.311E-07	17	10	104
Fe I	6355.040	2.845	3.802E-03	94		
Fe I	6358.690	0.859	3.404E-05	193		
Fe I	6380.750	4.186	3.981E-02	41		125
Fe I	6392.550	2.279	9.333E-05	38	57	152
Fe I	6393.600	2.433	2.399E-02	210	229	
Fe I	6408.02	3.690	1.000E-01	126		202
Fe I	6411.650	3.654	1.514E-01			163
Fe I	6421.350	2.279	9.397E-03	245		
Fe I	6430.850	2.176	9.863E-03	248		
Fe I	6494.980	2.404	5.333E-02	297		
Fe I	6498.950	0.958	2.000E-05	194		
Fe I	6518.380	2.832	1.778E-03	103	79	
Fe I	6551.680	0.990	1.622E-06			117
Fe I	6569.230	4.733	3.802E-01		54	
Fe I	6574.240	0.990	9.120E-06	137		218
Fe I	6575.020	2.588	1.514E-03	100	144	144
Fe I	6581.220	1.485	1.380E-05	99		160
Fe I	6591.320	4.593	8.511E-03	12		
Fe I	6592.910	2.728	2.512E-02	160	219	
Fe I	6593.880	2.433	3.784E-03	158	186	
Fe I	6597.610	4.796	8.511E-02	18		
Fe I	6608.030	2.279	9.333E-05	26	48	
Fe I	6609.120	2.559	2.032E-03	99	156	
Fe I	6646.960	2.609	1.023E-04	23		27
Fe I	6648.08	1.010	1.202E-06	67	50	101
Fe I	6665.47	1.560	2.042E-06	16		
Fe I	6667.420	2.453	3.981E-05	21		
Fe I	6677.990	2.692	3.388E-02		197	
Fe I	6703.570	2.759	6.918E-04	43	42	
Fe I	6705.10	4.610	5.248E-02	24		
Fe I	6710.310	1.485	1.318E-05	68	74	
Fe I	6715.410	4.608	2.291E-02	19		
Fe I	6739.540	1.557	1.122E-05	38		
Fe I	6745.110	4.580	6.918E-03		10	
Fe I	6750.150	2.424	2.393E-03	130	170	
Fe I	6752.720	4.638	4.365E-02	31	14	
Fe I	6786.880	4.191	8.511E-03	18	28	
Fe I	6806.850	2.728	6.166E-04	38		
Fe I	6810.280	4.607	7.586E-02	20		
Fe I	6841.350	4.607	1.778E-01	30		
Fe I	6842.670	4.638	4.786E-02	13		

Element	λ, Å	EP	log gf	W		
				S04103	S04603	S13011
Fe I	6851.640	1.608	4.786E-06	25		
Fe I	6855.16	4.560	1.514E-02	43		
Fe I	6855.740	4.607	1.514E-02	29		
Fe II	5325.560	3.221	2.512E-03			164
Fe II	5991.370	3.153	1.820E-04	71	72	
Fe II	6084.100	3.199	1.047E-04	46	29	
Fe II	6113.330	3.221	4.898E-05	41		50
Fe II	6149.250	3.889	1.202E-03	80		
Fe II	6238.38	3.889	1.349E-03	44	38	
Fe II	6247.550	3.892	3.090E-03	56	47	
Fe II	6383.720	5.553	5.370E-03	12		
Fe II	6416.920	3.892	1.413E-03	50	17	
Fe II	6432.680	2.891	1.820E-04	84	80	
Fe II	6516.080	2.891	3.548E-04	123	82	
Fe II	7515.790	3.903	2.089E-04	28	30	
Co I	5647.230	2.280	2.754E-02	37		
Co I	6116.990	1.785	3.236E-03	17		
Co I	6189.010	1.711	3.548E-03	26		
Co I	6429.910	2.137	3.890E-03	16		
Co I	6678.820	1.952	2.089E-03	8		
Co I	6771.040	1.883	1.072E-02	58		
Ni I	5578.720	1.676	2.291E-03	111	154	
Ni I	5587.870	1.935	7.244E-03	109		
Ni I	5593.740	3.898	1.445E-01	44		
Ni I	5641.880	4.105	8.511E-02	12		
Ni I	5682.200	4.105	3.388E-01	48		
Ni I	5748.340	1.676	5.495E-04	88	85	
Ni I	5754.680	1.935	4.677E-03	135	181	
Ni I	5796.092	1.950	2.075E-04	18	22	
Ni I	5847.000	1.676	6.166E-04	38	79	
Ni I	5996.740	4.236	8.710E-02	9	21	
Ni I	6007.310	1.676	4.677E-04	47	58	
Ni I	6086.290	4.266	2.951E-01	20	16	
Ni I	6108.120	1.676	3.548E-03	96		
Ni I	6111.060	4.088	1.349E-01		43	
Ni I	6175.420	4.089	2.951E-01	28	39	
Ni I	6176.810	4.088	2.951E-01	27	55	
Ni I	6177.260	1.826	3.162E-04	29		
Ni I	6191.186	1.680	2.244E-03	185		
Ni I	6223.990	4.105	1.023E-01	36	24	
Ni I	6322.170	4.154	6.761E-02	8		
Ni I	6327.600	1.676	7.079E-04	135	94	
Ni I	6360.818	4.170	6.546E-02		6	
Ni I	6378.260	4.154	1.288E-01	16		
Ni I	6482.800	1.935	2.344E-03	74	106	
Ni I	6532.890	1.935	4.074E-04	25	33	
Ni I	6586.330	1.951	1.549E-03	78	59	
Ni I	6772.360	3.658	1.047E-01	60	41	

Element	λ, Å	EP	log gf	W		
				S04103	S04603	S13011
Ni I	6842.070	3.658	3.311E-02	12		
Cu I	5105.545	1.390	3.090E-02			248
Cu I	5218.209	3.820	1.862E+00			113
Cu I	5782.136	1.640	1.660E-02	68	77	
Zn I	6362.352	5.790	1.871E+00			59
Y I	6023.410	0.000	1.413E-02	29		
Y I	6222.610	0.000	2.042E-02	52		
Y I	6435.049	0.070	1.500E-01	8		95
Y II	5289.820	1.033	1.400E-02			62
Y II	5320.782	1.084	1.169E-02			20
Y II	5402.770	1.839	2.344E-01			37
Y II	5728.888	1.839	7.499E-02	13		
Y II	6795.43	1.730	2.570E-02	14	22	
Zr I	5885.629	0.070	7.586E-03	15		
Zr I	5955.63	0.000	3.467E-02	28	27	
Zr I	6025.44	0.150	4.786E-02	8	9	
Zr I	6127.475	0.150	8.710E-02			46
Zr I	6134.570	0.000	5.248E-02	13		92
Zr I	6143.183	0.070	7.943E-02	41		58
Zr I	6762.36	0.000	8.128E-02	28	29	
Mo I	5751.420	1.420	1.067E-01	7		
Mo I	6030.660	1.530	3.589E-01	14		
Ba II	5853.668	0.604	1.000E-01	201	188	380
Ba II	6141.713	0.704	8.318E-01	328		640
Ba II	6496.897	0.604	4.169E-01			560
La II	5808.31	0.000	8.318E-03	19	15	
La II	6262.25	0.400	3.548E-02	11	29	64
La II	6390.48	0.320	3.256E-02	23	22	
La II	6526.95	0.230	2.630E-02	58	54	99
Ce II	5274.236	1.040	2.104E+00			70
Ce II	5610.24	1.040	1.000E+00		5	
Nd II	5089.831	0.205	6.761E-02			74
Nd II	5092.802	0.380	2.344E-01			84
Nd II	5293.169	0.823	8.710E-01			151
Nd II	5311.476	0.986	3.802E-01			71
Nd II	5319.820	0.550	6.166E-01			106
Nd II	5740.875	1.160	2.818E-01	10		
Nd II	5842.385	1.282	2.512E-01	7	39	
Nd II	6031.306	1.282	1.995E-01	26		
Nd II	6034.227	1.545	2.951E-01		12	
Eu II	6049.510	1.279	1.600E-01			62
Eu II	6437.640	1.320	5.297E-01	18		106
Eu II	6645.127	1.380	1.600E+00	44	37	83